



Research paper

Highly active Pt/Na_xTiO₂ catalyst for low temperature formaldehyde decompositionLei Wang^{a,b}, Haiqin Yue^{a,b}, Zelin Hua^{a,b}, Haoyi Wang^a, Xiaobao Li^{a,b}, Licheng Li^{a,b,*}^a College of Chemical Engineering, Nanjing Forestry University, Nanjing 210037, PR China^b Jiangsu Key Lab for the Chemistry & Utilization of Agricultural and Forest Biomass, Nanjing Forestry University, Nanjing 210037, PR China

ARTICLE INFO

Article history:

Received 1 May 2017

Received in revised form 9 July 2017

Accepted 25 July 2017

Available online 25 July 2017

Keywords:

HCHO oxidation

Platinum

TiO₂

Sodium

Adsorption

ABSTRACT

A series of titania nanowires containing different Na content (Na_xTiO₂) were prepared from sodium titanate by varying the pH value of ion-exchange. They were used to load the Pt nanoparticles for low temperature formaldehyde catalytic oxidation. As prepared samples were systematically characterized by X-ray diffraction (XRD), transmission electron microscope (TEM), X-ray photoelectron spectroscopy (XPS), in situ diffuse-reflectance infrared Fourier transform spectroscopy (DRIFTS), temperature programmed reduction/desorption/oxidation (TPR/TPD/TPO) and so on. The results showed that Na_xTiO₂ were consisted of anatase and sodium titanate. As pH value increased, the surface area and anatase content of catalyst decreased. Pt particles on Na_xTiO₂ were more easily oxidized and had smaller size but less exposed atoms compared with those on pure TiO₂. The HCHO catalytic oxidation result exhibited that Pt/Na_xTiO₂ catalysts possessed excellent HCHO catalytic oxidation at ambient temperature that were 8.9–52.8 times the activities as that of Pt/TiO₂. Kinetic studies manifested the easy activation of HCHO reaction over Pt/Na_xTiO₂ catalysts. Structure-performance analysis showed that the enhanced performance of Pt/Na_xTiO₂ catalysts was mainly attributed to two factors: increase in HCHO adsorption amount and change in HCHO decomposition pathway. According to HCHO-DRIFTS, linearly adsorbed CO generated from formate can react with hydroxyls to be carbonate/bicarbonate over Pt/Na_xTiO₂ catalysts. Simultaneously, the formate in Pt/Na_xTiO₂ catalyst with high Na content was also decomposed into a weak adsorbed CO. Both reaction pathways avoided the strong adsorption of CO on Pt/Na_xTiO₂ catalysts, which can facilitate the HCHO decomposition.

© 2017 Elsevier B.V. All rights reserved.

1. Introduction

Formaldehyde (HCHO) is one of the most representative indoor pollutants, which does great harm to the health of human beings [1]. In recent years, the HCHO elimination's hazard has attracted increased public attentions. Therefore, various techniques for removing HCHO were invented, including biodegradation, physical adsorption, chemical reaction, and so on. Catalytic oxidation, one strategy of the chemical reactions, was recognized as the most promising HCHO removal technology [2]. Among a great many candidates, the Pt-based catalysts possess the unparalleled HCHO oxidation catalytic activity, especially for that they can spontaneously oxidize formaldehyde to nontoxic CO₂ at ambient temperature without illumination of external energy [3,4]. How-

ever, Pt is the typical noble metal that always keeps expensive. Considered that the irreplaceable advantage of Pt in HCHO catalytic oxidation, it is expected to develop the more active and efficient Pt-based catalyst for reducing its own cost.

Firstly, attentions to optimize the preparation processes of Pt-based catalyst have been paid, for example Pt loading method, the reduction temperature, poisons [5–7]. Afterwards, the constituent of active sites of catalyst was focused on by most investigators. The general strategy was to incorporate other relatively cheap metals into Pt for synthesizing the multi-alloy, and the synergetic interaction between them was expected to improve the catalytic performance [8,9]. Nevertheless, this strategy seems to be not suitable for the development of Pt-based catalyst over the HCHO oxidation. In some literatures, alloyed Pt catalyst did not exhibit the prospective catalytic performance but instead turned worse [10–12]. Liu et al. even pointed out that, in the Pt-Au bimetal catalyst, it needed to avoid the alloying of two metals, and otherwise the obtained catalyst would have a low activity in HCHO oxidation [10]. In comparison, introduction of metal oxide into Pt-based catalyst

* Corresponding author at: College of Chemical Engineering, Nanjing Forestry University, Nanjing 210037, PR China.
E-mail address: llc0024@yahoo.com (L. Li).

can achieve a promotional effect on the HCHO oxidation performance, for example Fe_2O_3 , CeO_2 , MnO_2 , and so on [6,13,14]. These oxides, due to the reducibility, can utilize their lattice oxygen to participate in the reaction for increasing the oxidizability of catalysts. Recently, alkali-metals were found to be the perfect promoter for Pt-based catalyst towards the HCHO oxidation. He and his coworkers found the HCHO conversion at 30 °C of Pt/TiO₂ containing the alkali-metals (Li, Na, K) can reach up to around 100% compared with 20% of the pristine one. The enhancement in catalytic activity was attributed to the existence of abundant surface hydroxyls brought by alkali-metals, which can facilitate the decomposition of formate, an intermediate of HCHO oxidation [15]. Similar observation can also be appeared in the metal hydroxide-promoted Pt catalysts, such as AlOOH , $\text{Ni}(\text{OH})_2$, and so on [16,17].

On the other hand, the modification of catalytic support is an alternative approach for development of active HCHO oxidation catalyst. Some comparative studies showed that the Pt loading on TiO₂ had better HCHO activity than that on other supports [18]. TiO₂ not only possesses the similar reducibility as other metal oxides (e.g. CeO_2 [17,19], Fe_2O_3 , MnO_2 [20]) but also can take the electronic synergetic-interaction with active sites [21]. However, low surface area is an obvious defect of conventional TiO₂ as the catalytic support for applications. This not only can't guarantee the good dispersion of Pt particles but also is difficult to provide enough reaction zone that is related to adsorption or diffusion of reactants [22]. To overcome the disadvantage, numerous efforts have been devoted to improve textural properties of TiO₂ by various methods. In the past time, good results could be acquired by sol-gel technique and template technique, which were the most common methods for synthesizing the porous material [23,24]. Furthermore, hydrothermal synthesis of sodium titanate can also prepare a linear TiO₂ with high surface area via subsequent ion-exchange and dehydration [25]. Noteworthy is that the Na content in final product can be controlled by changing the ion-exchange process of sodium titanate [26]. Two advantages can be achieved for the prepared material as the catalytic support towards HCHO oxidation: high surface area and no use of external Na precursor. As mentioned above, alkali-metals have been demonstrated to be beneficial to the improvement in HCHO oxidation. Accordingly, the linear TiO₂ containing Na supported Pt catalyst would have an excellent catalytic oxidation performance due to a combination effect of large reaction interface and abundant hydroxyls.

Therefore, in the present work, a series of TiO₂ nanowires containing different Na content (Na_xTiO_2) derived from sodium titanate were prepared by controlling the pH value of ion-exchange. As-prepared materials were used to load Pt particles for HCHO oxidation. The structural and physicochemical properties of various catalysts were systematically analyzed by TEM, BET, TPR/O, CO-DRIFTS, and so on. Simultaneously, the structure-performance relationship was also studied by HCHO-TPD and in-situ DRIFTS.

2. Experimental

2.1. Materials and synthesis

Chloroplatinic acid ($\text{H}_2\text{PtCl}_6 \cdot 6\text{H}_2\text{O}$, Shanghai Agent Co., Ltd), commercial titanium dioxide (TiO₂, Degussa), sodium hydroxide (NaOH, Nanjing Agent Co., Ltd), nitric acid (NaOH, Nanjing Agent Co., Ltd), Trioxane (Macklin agent Co., Ltd) were used as received.

Na_xTiO_2 was synthesized by hydrothermal treatment following a procedure reported in reference [21]. Firstly, 1 g of TiO₂ (P25) was dispersed in 40 ml of 10 M NaOH aqueous solution in Teflon lining. Then, put the mixed suspension in homogeneous reactor. After treatment at 130 °C for 48 h, the mixture was cooled down to room temperature and the supernatant was discarded to acquire

the sodium titanate. For ion-exchange process, the sodium titanate was dispersed in deionized water (~100 ml water/g sodium titanate) and the pH values was adjusted to 2, 4, 6 and 8 by 1 M HNO_3 aqueous solution. With stirring at room temperature for 2 h, the powders was collected and dried at 80 °C to obtain the hydrated titanate.

Loading of Pt particles (0.5 wt%) was carried out by wet impregnation using $\text{H}_2\text{PtCl}_6 \cdot 6\text{H}_2\text{O}$ as the precursor. The hydrated titanate prepared by different pH value were impregnated with $\text{H}_2\text{PtCl}_6 \cdot 6\text{H}_2\text{O}$ aqueous solution, followed by drying at 110 °C for 12 h and sequent calcinations at 500 °C for 2 h. Finally, the powders were reduced in 10% H_2/N_2 at 300 °C for 2 h to acquire the Pt/ Na_xTiO_2 catalyst that expressed as Pt/ NaTx , x was the pH value of ion-exchange process.

2.2. Characterization

The crystal structure of the samples was characterized by X-ray diffractometer (XRD, Bruker D8 Advance) with Cu K α radiation at a scanning rate of 10°/min and a step size of 0.02°. Nitrogen adsorption/desorption (at –196 °C) were performed by using the ASAP 2020 system (Micromeritics, USA). Surface area (S_{BET}) and pore volume (V_p) was obtained by BET method and nitrogen adsorption at a relative pressure of 0.99, respectively. Pore size distributions were found from adsorption isotherms by BJH method. The morphology of the samples was observed by scanning electron microscopy (SEM, JEM-7600F) at 15 kV with attached Oxford Instruments' X-ray energy-dispersive spectroscopy (EDS) system. The size and morphology of Pt particles was further observed by transmission electron microscopy (TEM, JEM-2010 UHR). X-ray photoelectron spectroscopy (XPS, ESCALAB 250) equipped with a monochromatic Al K α X-ray beam (1486.6 eV) was used to analyze the chemical state of Pt, O and Na on the catalyst surface. All binding energies were referenced to the C1 s peak (284.6 eV) arising from the adventitious hydrocarbons. The exposed surface area of Pt particles was determined by pulse adsorption with CO as adsorbate (AutoChem II 2920). The catalyst was firstly reduced by 10% H_2/N_2 at 300 °C for 2 h. After cooling down to room temperature, the chemisorption was performed at 50 °C using 1% CO/He.

Temperature programmed experiments in present work contain the temperature programmed reduction (TPR), the temperature programmed oxidation (TPO) and the temperature programmed desorption (TPD). TPR experiments were conducted by using the TP-5000 equipment. The sample was preliminarily oxidized at 500 °C by 5% O_2/He . Then, the test temperature was increased from room temperature up to 400 °C at a rate of 10 °C/min. The gas mixture of 10% H_2/N_2 was introduced at 30 ml/min into the quartz reactor and that was also used as a reference gas. TPO experiments were also carried out in this equipment. The sample was pretreated by 10% H_2/N_2 at 300 °C, and then oxidized by 5% O_2/He at programmed temperature from room temperature up to 500 °C at a rate of 10 °C/min. For HCHO-TPD experiments, the sample was pretreated in He at 300 °C for 1 h and then cooled down to room temperature. The HCHO were produced by catalytic thermal depolymerization of trioxane vapor generated from diffusion tube, which were constantly pulsed into the test tube. After the adsorption of HCHO was saturated, the temperature was ramped from room temperature to 400 °C at a rate of 10 °C/min with the pure He gas flowing at a rate of 30 ml/min.

In situ diffuse reflectance infrared Fourier transformed spectroscopy (in situ DRIFTS) was carried out on a Nicolet-360 spectroscope apparatus (Thermo Electron) equipped with a diffuse reflectance accessory and a MCT detector. DRIFTS test can be divided into HCHO-DRIFTS and CO-DRIFTS depending on different adsorbate. The HCHO-DRIFTS operational processes were taken to study the possible reaction path of formaldehyde oxidation. As prepared samples were placed in a ceramic crucible of the

in situ chamber and smoothed out. Firstly, the catalyst was pre-treated from room temperature to 300 °C at a rate of 10 °C/min and then cooled down to room temperature in a pure He flow of 30 ml/min. Then, HCHO vapor were introduced into the chamber at 30 °C for 1 h. The pure He and 20% O₂/He passed through the chamber sequentially to study the consumption and oxidation of different intermediate. The spectra under reaction conditions were recorded after 32 scans with a resolution of 4 cm⁻¹. The CO-DRIFTS can analyze the dispersion state of Pt particles. The catalyst was reduced in 10% H₂/N₂ at 300 °C for 0.5 h and cooled down to room temperature in He flow. CO were introduced into the chamber at 30 °C for 0.5 h and excessive and weakly adsorbed CO was removed by purged by a flowing pure He stream. Also, the spectra under reaction conditions were recorded after 32 scans with a resolution of 4 cm⁻¹.

2.3. Catalytic activity test

The formaldehyde oxidation reaction was operated in a fixed bed flow reactor. 0.1 g of catalyst was filled in quartz tube ($D=8$ mm). Formaldehyde was produced by passing a stream of the pure N₂ through a bubbler containing a 37% HCHO aqueous solution in bath at 4 °C. The total flow of feed gas was 75 ml/min (GHSV = 45,000 ml h⁻¹ g⁻¹), containing 400 ppm of formaldehyde and 35% relative humidity balanced with air. The reaction temperature was controlled by a shaft furnace from 30 to 140 °C. Formaldehyde conversion was calculated according to the change in HCHO concentration between the inlet and outlet gases. The initial and exhaust HCHO concentration was analyzed online by gas chromatograph. In addition, the kinetics studies of various catalysts were carried out to calculate the intrinsic reaction rate (r_M), turnover frequencies (TOFs) and apparent activation energy (E_a). Kinetics data were tested under the condition of HCHO 400 ppm and GHSV 45000 ml h⁻¹ g⁻¹ for Pt/TiO₂, HCHO 650 ppm and GHSV 105000 ml h⁻¹ g⁻¹ for Pt/NaT8, and HCHO 650 ppm and GHSV 210000 ml h⁻¹ g⁻¹ for Pt/NaT2, Pt/NaT4 and Pt/NaT8.

3. Results and discussion

3.1. Structural properties of supports

XRD was preliminarily used to study the crystal structure of various catalysts. Fig. 1(a) shows five strong diffraction peaks at $2\theta=25.4^\circ$, 37.8° , 49.7° , 53.9° and 55.1° in all samples, which is assigned to the anatase phase. Moreover, there are three peaks at $2\theta=27.5^\circ$, 36.1° and 41.2° ascribed to the rutile phase in the control sample Pt/TiO₂ [27]. No diffractive signals of Pt species are appeared in the XRD spectra, suggesting Pt nanoparticles are sufficiently well dispersed in all catalysts. Besides the characteristic peaks of anatase phase, the pattern of Pt/NaT8 exists new peaks vibrated at $2\theta=24.5^\circ$, 29.6° , 33.0° and 43.9° , which are corresponding to (110), (111), (-310) and (003) planes of Na_{0.23}TiO₂ [28,29]. The intensity of peak at $2\theta=24.5^\circ$ is the most remarkable. It can also see the weak characteristic peaks of Na_{0.23}TiO₂ in the pattern of Pt/NaT6, while hardly observe them in Pt/NaT2 and Pt/NaT4. Fig. 1(b) displays the differentiation imitating analysis result of diffraction peak between $2\theta=23.5^\circ$ and 26.5° . The diffraction peak of Pt/Na_xTiO₂ catalysts can be resolved into two peaks ascribed to (101) plane of anatase and (110) plane of Na_{0.23}TiO₂, respectively. The peak intensity of Na_{0.23}TiO₂ gradually gets more obvious as pH value increases that mean the increasing content of Na_{0.23}TiO₂ phase in the Pt/Na_xTiO₂ catalyst, as also reflected by the Na content in Table 1. Thus, the supports of Pt/Na_xTiO₂ catalysts are consisted of the hybrid phase of anatase and sodium titanate so that they can be expressed as Na_xTiO₂.

Table 1

Textural characteristics and sodium content of Pt/Na_xTiO₂ catalyst.

Catalyst	S_{BET} (m ² /g)	V_p (cm ³ /g)	D_p (nm)	Na content α (wt%)
Pt/NaT2	107.3	0.76	21.2	2.52
Pt/NaT4	78.1	0.74	16.8	3.83
Pt/NaT6	66.9	0.51	15.8	8.98
Pt/NaT8	26.0	0.15	13.7	9.57
Pt/TiO ₂	40.1	0.40	19.5	–

α : Na content here was detected by XPS.

Fig. 2 shows the morphology of Pt/Na_xTiO₂ catalysts and the control sample Pt/TiO₂. Nanowires can be remarkably observed in all Pt/Na_xTiO₂ catalysts while nanoparticles in Pt/TiO₂. Especially for Pt/NaT2, it is constituted by the uniform size wires and their lengths are longer than 2 μ m (seen in Fig. 2(a)). As the pH value of ion-exchange increases, slight nanoparticles arise in Pt/Na_xTiO₂ catalysts, and simultaneously their length-diameter ratio of wires decreases. A substantial number of nanowires are agglomerated together in Pt/NaT8 (seen in Fig. 2(d)). Up to now, no agreement on the transformation mechanism of TiO₂ powders into wires was reached. The debate was mainly focused on which process, either hydrothermal or ion-exchange, to influence the morphology of nanostructured titania [30]. So many influence factors lead to the complexity and abstruseness of morphology transformation. Anyhow, it can be confirmed here that pH value of ion exchange influences both Na content and length of NaTiO₂.

N₂ adsorption-desorption isotherms of various catalysts are displayed in Fig. 2(f). Clearly, Pt/Na_xTiO₂ catalysts possess the mesoporous structure, identical to control sample Pt/TiO₂ does. This is due to the type IV isotherm characteristic for each catalyst [31], and the corresponding average pore size are listed in Table 1. Pt/NaT2 has a led specific surface area of 107.3 m²/g and pore volume of 0.74 cm³/g compared with other catalysts. The Pt/Na_xTiO₂ catalyst with high pH value has low quality of N₂ adsorption in the isotherm, suggesting the small surface area and low porosity. The specific surface area of Pt/NaT4 and Pt/NaT6 are 78.1 m²/g and 66.9 m²/g, respectively. Apart from Pt/NaT8 catalyst, Pt/Na_xTiO₂ catalysts have superior porous structure compared with that of control sample Pt/TiO₂.

3.2. Dispersed states of Pt nanoparticles

The representative HRTEM images and derived Pt particle size distributions of Pt/Na_xTiO₂ catalysts are displayed in Fig. 3. All the Pt particles can be well dispersed on the surface of Na_xTiO₂ and TiO₂, which are in accordance with the analysis result of XRD. In the right of graphs, it can be seen that all the Pt particles are spherical or hemispherical in shape. The average Pt particle size of Pt/TiO₂ is 2.62 nm. In comparison, the Pt particles loaded on Na_xTiO₂ display smaller size, e.g. the average size of NaT2 is approximately 1.98 nm. As pH value increases, the Pt/Na_xTiO₂ catalyst has the Pt particles with smaller size. The average size decreases to only 1.64 nm in Pt/NaT8. However, it can be clearly seen that the decrease in Pt particle size of Pt/Na_xTiO₂ is not accompanied with increasing their surface areas. That is to say the improvement in the Pt dispersion of Na_xTiO₂ catalysts should not be mainly related to the surface area of various catalysts. Thus, the surface properties due to different preparation are the only explanation left responsible for the Pt dispersion of catalyst. As shown in Fig. 3(h), well resolved lattice fringes corresponding to anatase TiO₂ and Na_{0.23}TiO₂ can be observed in Pt/NaT8 catalyst, proving the presence of sodium titanate phase on the surface of NaT8. With respect to other Pt/Na_xTi_{1-x}O₂ catalysts, no Na_{0.23}TiO₂ phase is observed in visible area of image. Even so, this can't demonstrate the absence of Na species on the surface of these Pt/Na_xTiO₂ catalysts. It is known

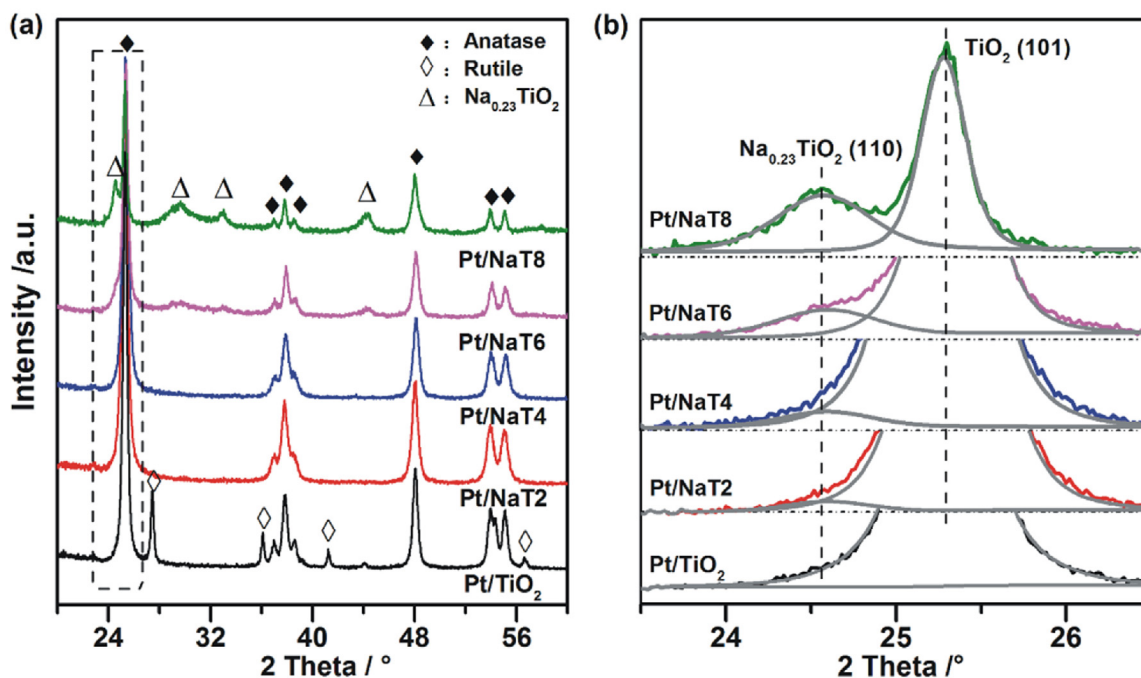


Fig. 1. (a) XRD patterns of Pt/Na_xTiO₂ catalysts and (b) the magnified version of the patterns at between 23.5° and 26.5°.

the XPS detection depth is generally limited to several nm. That means the Na species, the content of which are listed in Table 1, overall disperse on the surface layer of various catalysts. According to XRD results, the Na species are existed on various Pt/Na_xTiO₂ catalysts in form of titanate, of course, also including the free NaO_x species. Therefore, the presence of Na species on Na_xTiO₂ surface should be the reason for variation in Pt particle size compared with that of pure TiO₂.

Mallinson et al. used the co-impregnation of Pt with NaNO₃ on the TiO₂ to prepare the Pt–Na/TiO₂, and found the average particle size of Pt increased when incorporation of Na species [32]. However, He et al. achieved the opposite experimental phenomenon. The dispersion of Pt particle on TiO₂ was greatly improved in the alkali-metal (Na or Li)-promoted Pt/TiO₂ and even appeared to be some single Pt atoms although they only used Na₂CO₃ instead of NaNO₃ [15]. By far, researchers could not reach an agreement on the influence of Na species on the Pt dispersion state. Herein, the dispersion of Pt particles in Pt/Na_xTiO₂ is substantially better than that in Pt/TiO₂. Different from other experiments, Pt particles in this study are directly deposited on the Na-containing titanate surface rather than on pure TiO₂ surface. A hypothesis is proposed that the Pt precursors, chloroplatinic acid, are preliminarily in contact with the Na_xTiO₂ surface. The Pt particles may be nucleated more rapidly since the superficial alkalinity as like the acid-base interaction of ion-exchange process. After heat treatment, the Na_xTiO₂ supported catalyst with good Pt dispersion can be achieved.

The similar result on the dispersion state of Pt particles can be further confirmed by in situ CO-DRIFTS. Fig. 4 displays that all the catalysts have two distinct bands at 2056 and 2078 cm^{−1}, which are assigned to the CO linearly adsorbed on Pt terrace and step sites, respectively [33–35]. This suggests that, in agreement with TEM analyses, Pt/Na_xTiO₂ catalysts and Pt/TiO₂ have similar morphology of Pt particles. Moreover, there is a shoulder band at below 2400 cm^{−1} observed in each catalyst, of which Pt/Na_xTiO₂ catalyst is red shifted with the increase in pH value. The shoulder band can be attributed to the CO adsorbed on very small Pt particles. The shift to lower frequencies of CO adsorption is explained by the decrease in Pt coordination that means the smaller particles size

of Pt [36,37]. This is also in accordance with the statistical result of Pt particle size derived from TEM images. However, the catalysts with higher pH value show lower peak intensity of CO adsorption, suggesting the worse Pt dispersion. CO titration results in Table 2 also exhibits the decreasing amount of the exposed Pt atoms in Pt/Na_xTiO₂ catalysts, which is in turn opposed to the result of TEM analysis. Mallinson et al. found that the NaO_x species can spontaneously migrate onto the Pt surface leading to formation of a novel strong metal-promoter interaction [32]. All catalysts in the present work have same Pt loading amount. Thus, the fewer amounts of exposed Pt atoms in Pt/Na_xTiO₂ catalysts compared with that in Pt/TiO₂ are probably due to the partial coverage of free NaO_x species over the Pt particles.

The electronic valence state of Pt particles was examined by XPS. The high-resolution XPS spectra of Pt4f, O1s and Na1s regions are shown in Fig. 5. All spectra of Pt/Na_xTiO₂ catalysts and Pt/TiO₂ (seen in Fig. 5(a)) display three 4f_{7/2}–4f_{5/2} doublets at binding energies of 70.5–72.0 eV, 72.1–72.9 eV and 74.4–75.0 eV are corresponding to Pt⁰, Pt²⁺ and Pt⁴⁺ species, respectively [44]. Their relative intensities were used to evaluate the metallic Pt⁰ content of Pt particles in various catalysts and the results were summarized in Table 3. Note that the presence of cationic Ptδ⁺ in the reduced catalyst can't be excluded due to the exposure in air and oxidation by O₂ or moisture during the transfer of catalyst to the XPS chamber. At least in part, the low Pt⁰/(Pt⁰ + PtO_x) value can manifest the easy oxidation for Pt particles. It is clearly seen that all the Pt/Na_xTiO₂ catalysts have lower contents of metallic Pt compared with Pt/TiO₂ does. The charge transfer from Pt to adjacent Ti of support can be excluded due to the low electro-negativity of Ti. As described previously, alkali metal could stabilize the Pt through Pt–O–M bond that made Pt particles liable to be oxidized [15]. Fig. 5(b) shows the Na1s XPS spectra of various Pt/Na_xTiO₂ catalysts. The peak located at 1071.1 eV is relevant to free NaO_x species, for example NaOH, Na₂CO₃ or NaHCO₃ [45,46], and the peak height increases with increasing pH value of Pt/Na_xTiO₂ catalyst. Moreover, two weak shoulders located in both sides of the peak can be observed, which are assigned to the formation of NaO_xC_y species (1067.3 eV) and the –O–Na linkage (1072.4 eV) that stabilizes the Pt atoms [47].

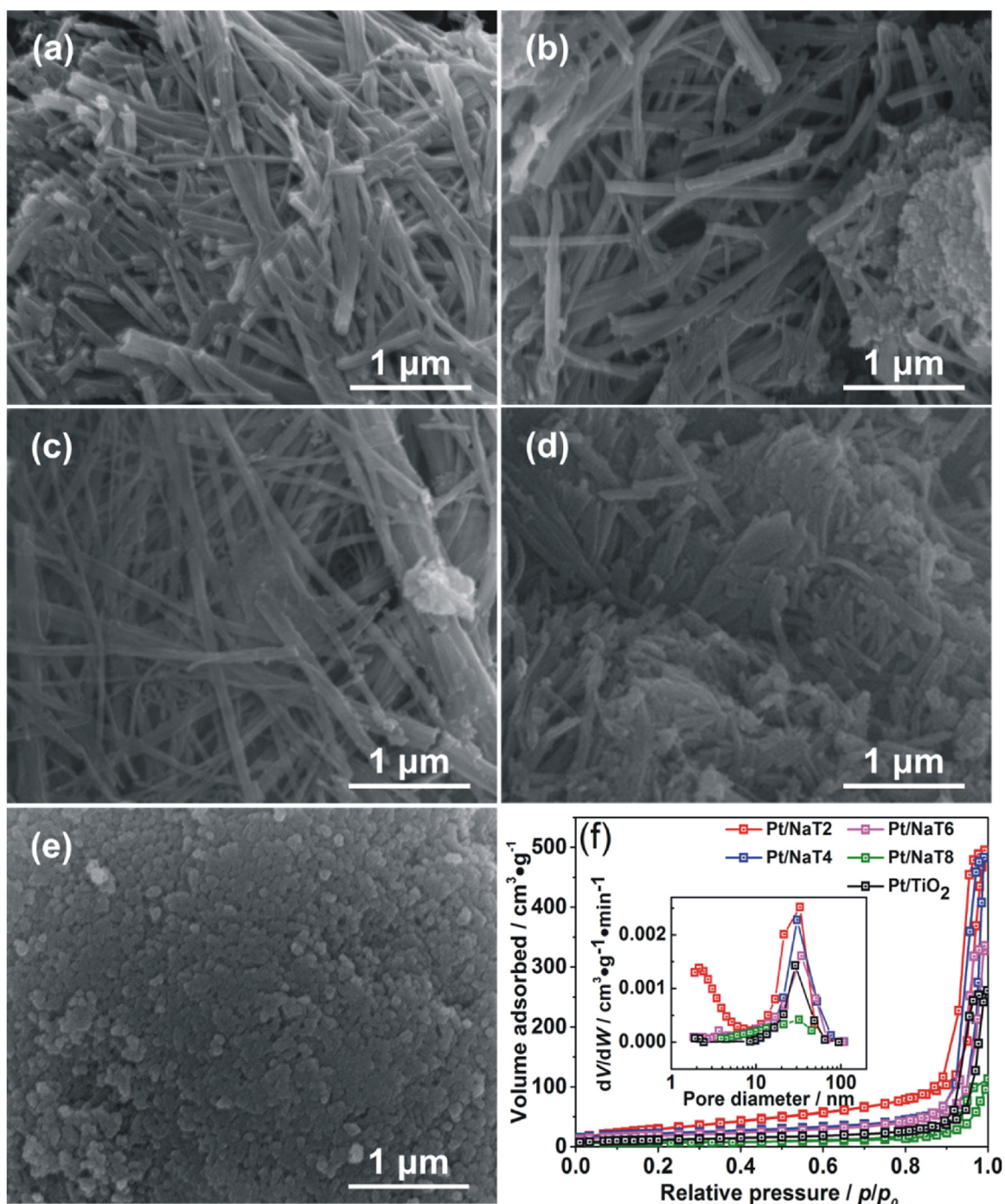


Fig. 2. SEM images of (a) Pt/NaT2, (b) Pt/NaT4, (c) Pt/NaT6, (d) Pt/NaT8 and (e) Pt/TiO₂, and (f) Nitrogen adsorption/desorption isotherms (inset: pore size distribution) of different Pt/Na_xTiO₂ catalysts.

Apparently, a fraction of Na species can interact with Pt particles as a result of high cationic Ptδ⁺ proportion in Pt/Na_xTiO₂ catalysts.

Oxygen species on the surface of catalyst is another key factor for influencing the HCHO oxidation, and the corresponding XPS spectra are displayed in Fig. 5(c). Each spectrum can be resolved into three peaks, which are corresponding to three kinds of oxygen species in the catalyst. They located at 529.5–530.0 eV, 531.7–532.0 eV and 533.4–533.6 eV, ascribed to lattice oxygen of bulk TiO₂ (O_I) of Na_xTi_{1-x}O₂, surface oxygen species (O_{II}) and surface hydroxyl oxygen, respectively [35]. Among them, O_{II} species and surface hydroxyl are considered to participate in the catalytic cycle, which

is important for decomposition of formaldehyde intermediates. As shown in Table 3, the O_{II}/O_I proportion of Pt/Na_xTiO₂ catalysts are overall lower than that of Pt/TiO₂, and in turn the OH⁻/O_I ratio of them have opposite comparison relationship that means the better ability to adsorb moisture for Pt/Na_xTiO₂ catalysts.

Based on above characterization analyses, H₂-TPR and O₂-TPO were jointly used to investigate the redox potential of Pt particles that loaded on Na_xTiO₂. Fig. 6(a) shows the H₂-TPR profiles of Pt/Na_xTiO₂ catalysts as a function of pH values. The solid lines represent the TPR profiles of Pt/Na_xTiO₂ catalysts and the dashed lines are the corresponding support's reduction results. It can be seen

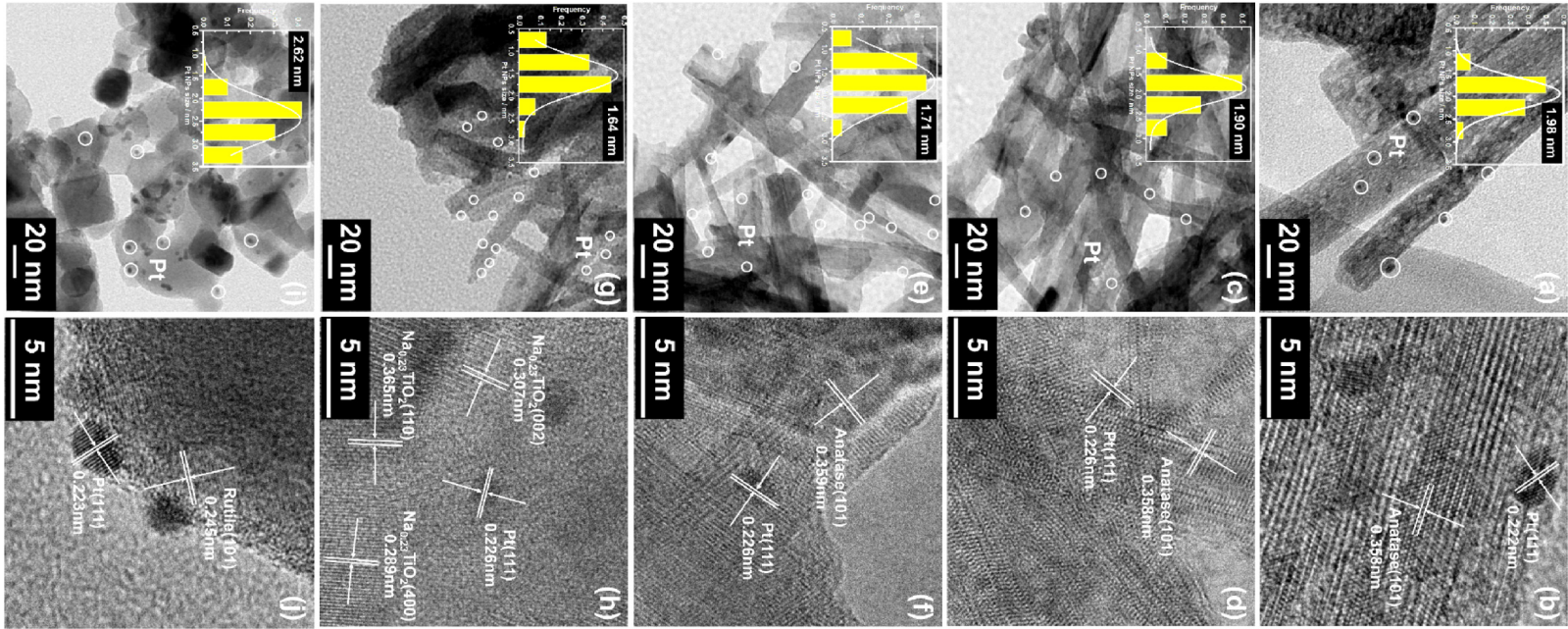


Fig. 3. HRTEM image of (a) Pt/NaT2, (c) Pt/NaT4, (e) Pt/NaT6, (g) Pt/NaT8, (i) Pt/TiO₂, and the right (b, d, f, h, j) are the magnified HRTEM image that corresponds to left HRTEM image. The inset figure is the size distribution of Pt particles over each catalyst.

Table 2
Comparison of catalyst activity with literature reports in formaldehyde oxidation.

Catalyst	Loading (wt%)	C ₀ (ppm)/GHSV (ml h ⁻¹ g ⁻¹)/Humidity (%)	T _{100%α} (°C)	E _a (kJ/mol)	r _{MB} (μmol _{HCHO} g _{cat} ⁻¹ s ⁻¹)	Surface metal atoms γ × 10 ⁻⁵ (mol g _{cat} ⁻¹)	TOF (s ⁻¹) × 10 ³	References
Pt/NaT2	0.5	650/210000/35	80	26.0	0.722	1.13	63.9	This work
Pt/NaT4	0.5	650/210000/35	120	22.4	0.300	1.30	23.1	This work
Pt/NaT6	0.5	650/210000/35	60	6.62	0.845	0.86	98.3	This work
Pt/NaT8	0.5	650/105000/35	120	3.97	0.142	0.45	31.6	This work
Pt/TiO ₂	0.5	400/45000/35	100	45.4	0.016	0.93	1.72	This work
Pt/TiO ₂	1	400/80000/50	R.T.(10 ppm)	–	0.029	1.37	2.12	[38]
Na-Pt/TiO ₂	1	700/300000/50	25	13 ± 4	–	–	–	[15]
Pd/TiO ₂	0.5	400/120000/50	R.T.(10 ppm)	–	0.088	2.84	3.12	[39]
Na-Pd/TiO ₂	1	140/190000/35	50	–	0.301	3.10	9.70	[40]
K-Pd/TiO ₂	1	550/640000/30	50	–	1.790	4.41	40.5	[41]
K-Ag/Co ₃ O ₄	1	2000/165000/50	70	28.5	0.037	1.41	2.62(100 °C)	[42]
Pt/MnO ₂ /TiNT	0.16	50/30000/35	60	–	0.019	–	–	[43]

α: T_{100%} is the reaction temperature as formaldehyde be decomposed completely.
 β: Calculated from the result of kinetics studies at 30 °C.
 γ: Obtained from CO titration (Table S2 in ESI).

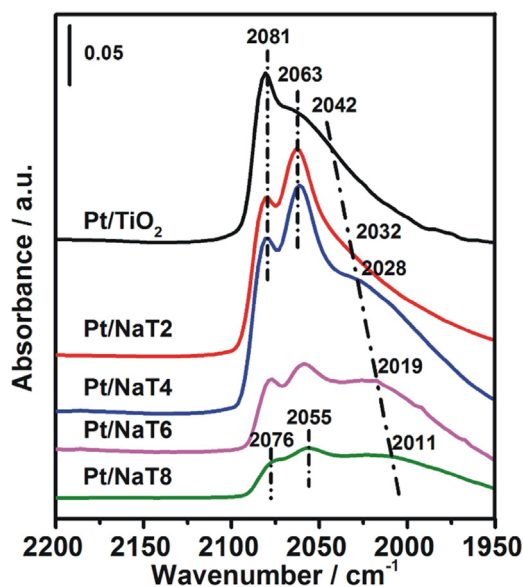


Fig. 4. CO-DRIFTS spectra of Pt/Na_xTiO₂ catalysts and Pt/TiO₂.

that the reduction process of all catalysts contain two stages, which are roughly divided into low temperature (<250 °C) and high temperature (>250 °C), corresponding to the reductions of Pt^{δ+} species [32,48] and of Na species plus TiO₂ species [49], respectively. Under the present conditions, some easily reduced Pt species (weak interaction with the support or ultra-small particle size [15,32]) may have been reduced at ambient temperature during the period of the TCD signal stabilization and thus do not appear at all. In low temperature region, the reduction peak of Pt/TiO₂ reaches a maximum at 93 °C. By comparison, Pt particles on the Na_xTiO₂ require the relatively high temperature for reduction that all corresponding peaks are located at the temperature range of 94–121 °C. This suggests the stronger interaction between Pt particles and Na_xTiO₂ compared with that of Pt/TiO₂. Unlike the pure TiO₂ with external Na species, Pt particles of Pt/Na_xTiO₂ may be loaded on the titanate rather than on TiO₂ so that the interaction mechanism of them changes. Similar observation can also be appeared in the reduction of other metals on titanate [50,51]. As pH value of Pt/Na_xTiO₂ catalysts increases, the reduction peak of Pt particles gradually shifts towards the low temperature, which may be caused by the decrease in the Pt particle size [52], as also evidenced by TEM.

Furthermore, the TPO data provides additional information on the redox properties of Pt particles (seen in Fig. 6(b)). The aforementioned XPS analysis result has demonstrated the existence of cationic Pt^{δ+} in the reduced catalysts once they are exposed in air or moisture. Thus, it is deduced that the superficial and interfacial Pt atoms between Pt particles and the support are liable to be preliminarily oxidized during the TCD signal stabilization. The core atoms of Pt particles can maintain to be metallic due to the disconnection with oxygen. As plotted in Fig. 6(b), the profiles of Pt particles on Na_xTiO₂ start to upwrap at around 120 °C, indicating the oxidation take places. The maximum in temperature of oxidation peaks are located at 196–257 °C. For Pt/TiO₂, the oxidation signal starts at 200 °C and the peak temperature is also at 257 °C. Significantly, the Pt particles on Na_xTiO₂ are more easily oxidized than those on TiO₂, in line with above analysis results of TPR and XPS.

3.3. Catalytic performance

The HCHO conversion over Pt/Na_xTiO₂ catalysts and Pt/TiO₂ together with pure TiO₂ and NaT6 as a function of reaction temperature are presented in Fig. 7(a). Pure TiO₂ and NaT6 have no activity for HCHO oxidation at the temperature of 30–120 °C even though they undergo the reduction. Analogously, the Pt/TiO₂ also has a low HCHO conversion at room temperature (30 °C) that is merely 4%. As the temperature increases, the catalytic activity of Pt/TiO₂ can be sharply improved, over which the complete conversion of HCHO is achieved at the temperature (T_{100%}) of 100 °C. Noteworthy is that Pt particles on Na_xTiO₂ exhibit the extremely excellent activities for oxidizing the HCHO. Especially for Pt/NaT6, the starting HCHO conversion can reach up to 90% and T_{100%} is at only 60 °C. The HCHO conversion sequence at 30 °C of studied catalysts is Pt/NaT6 > Pt/NaT2 > Pt/NaT4 > Pt/TiO₂. The intrinsic reaction rate (r_m) summarized in Table 2 can provide quantificational comparison in the activity over different catalysts. A series of Pt/Na_xTiO₂ catalysts possess 8.9–52.8 times the activities as that of Pt/TiO₂, which also have advantage in catalytic performance compared with other catalysts reported in literatures. The promotional effect on catalytic performance of Pt/Na_xTiO₂ can be explained by the formation of new active sites due to the different TOF values. According to the long-time isothermal test (as seen in Fig. 7(b)), the chosen catalyst, Pt/NaT6, does not appear any deactivation after 72 h of continuous reaction, implying the good catalytic stability of Pt/Na_xTiO₂ catalysts.

Furthermore, the Arrhenius plots of intrinsic reaction rate over different Pt/Na_xTiO₂ catalysts in the reaction temperature range of 10–60 °C are displayed in Fig. 8. The apparent activation ener-

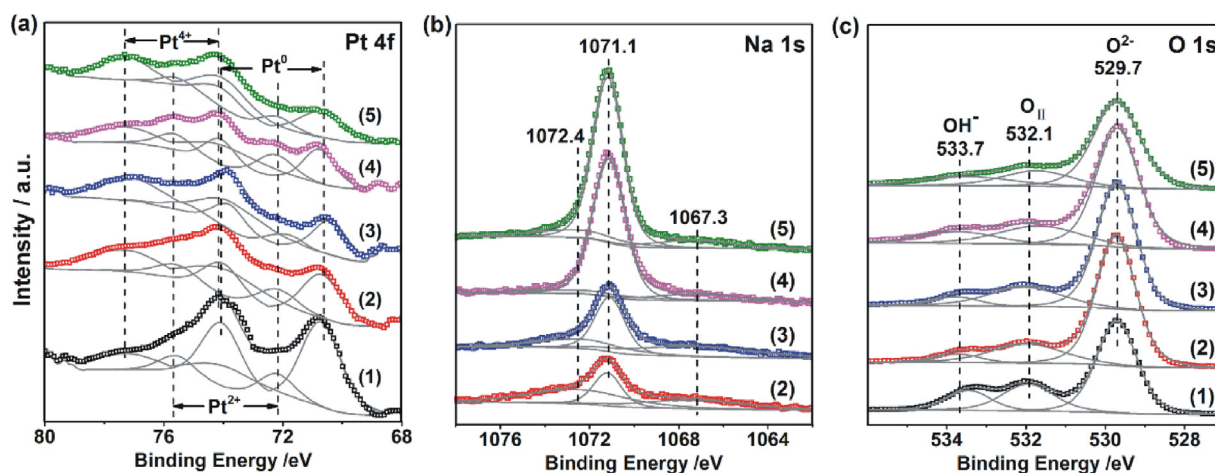


Fig. 5. XPS spectra of Pt/Na_xTiO₂ catalysts and Pt/TiO₂: (a) Pt 4f and (b) Na 1s and (c) O 1s. Each inset profile: (1) Pt/TiO₂, (2) Pt/NaT2, (3) Pt/NaT4, (4) Pt/NaT6 and (5) Pt/NaT8.

Table 3
XPS data of Pt/ Na_xTiO_2 catalysts and Pt/ TiO_2 .

Catalyst	BE of Pt^0 4f _{7/2} /eV	$\text{Pt}^0/(\text{Pt}^0 + \text{PtO}_x)/\%$	BE of O_I 1s _{1/2} /eV	O_{II}/O_I	OH^-/O_I
Pt/NaT2	70.9	44.1	529.5	0.275	0.069
Pt/NaT4	71.0	39.0	529.4	0.284	0.080
Pt/NaT6	70.6	36.1	529.5	0.296	0.176
Pt/NaT8	70.6	37.2	529.9	0.255	0.203
Pt/ TiO_2	71.3	58.2	529.7	0.301	0.052

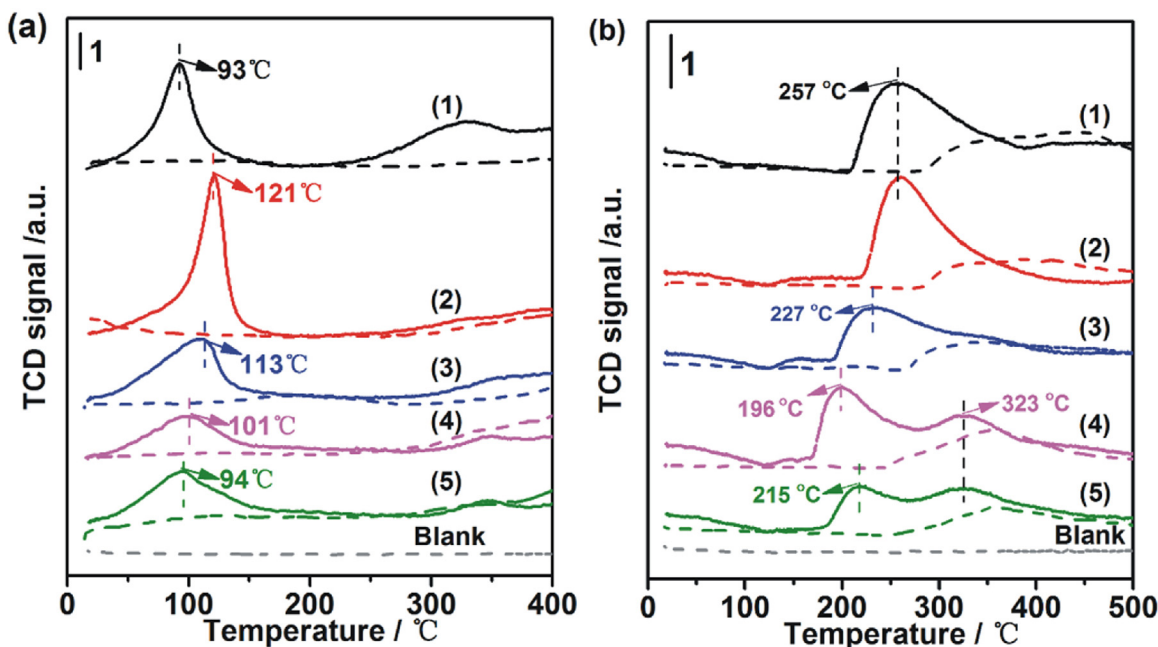


Fig. 6. (a) TPR profiles, (b) TPO profiles of Pt/ Na_xTiO_2 and Pt/ TiO_2 catalysts. The dotted lines in the patterns are the TPR or TPO results of corresponding supports without Pt nanoparticles. Each inset profile: (1) Pt/ TiO_2 , (2) Pt/NaT2, (3) Pt/NaT4, (4) Pt/NaT6 and (5) Pt/NaT8.

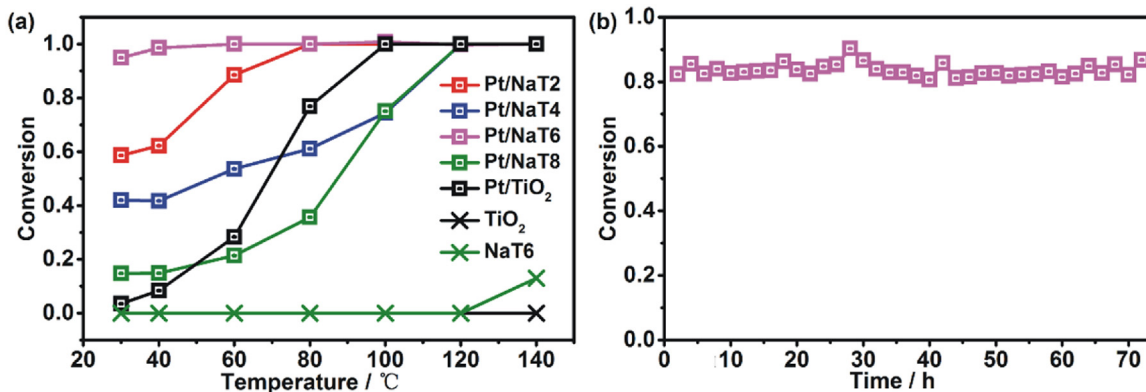


Fig. 7. (a) Formaldehyde oxidation performance of Pt/ Na_xTiO_2 catalysts and corresponding support. (b) Stability test of Pt/NaT6.

gies (E_a) for the HCHO oxidation reaction are obtained from the fitted slopes in Fig. 8 and reported in Table 2. Clearly, the E_a of Pt/ Na_xTiO_2 catalysts are 3.97–26.0 kJ/mol, overall lower than that of Pt/ TiO_2 (45.4 kJ/mol), implying the HCHO oxidation reaction are easier to activate. The different E_a between Pt/ Na_xTiO_2 catalysts and Pt/ TiO_2 indicate their varying reaction pathway of HCHO, as also reflected by TOF analysis. Furthermore, the E_a of Pt/ Na_xTiO_2 catalysts together with intrinsic reaction rate does not monotonously increase or decrease with increasing pH value. Based on above-mentioned analyses, it is deduced that there may be several factors jointly influencing the final HCHO oxidation performance of catalysts. Therefore, the following discussion in the next part of context

is focused on the relationship between structure and performance of Pt/ Na_xTiO_2 catalysts.

3.4. Discussion

From the comprehensive characterization results mentioned above, it can be seen that the pH value of ion exchange in the Na_xTiO_2 preparation process influences many subsequent structural characteristics of its own, including the surface area, morphology, crystalline phase of support and the particle size, valence state, redox performance of Pt particles, and so on. One or some of them may be the key factor for influencing final catalytic

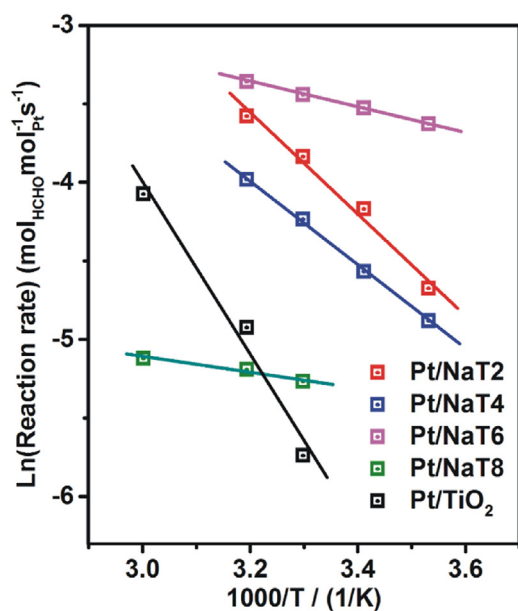


Fig. 8. Arrhenius plots of the reaction rate for HCHO oxidation over Pt/Na_xTiO₂ catalysts.

performance. Therefore, it is necessary to dissect the influence mechanism of respective factor on the HCHO oxidation performance of catalyst.

As shown in Table 1 and Fig. 2, the support of Pt/Na_xTiO₂ catalyst has the essentially structural difference from that of Pt/TiO₂, which is attributed to their different synthetic route. TiO₂ is shaped in granular form but Na_xTiO₂ has the linear structure. The surface areas of Pt/Na_xTiO₂ catalysts, except Pt/NaT8, are larger than that of Pt/TiO₂. For crystalline and constitution, Pt/Na_xTiO₂ catalysts are consisted of sodium titanate and anatase, whereas anatase and rutile phase for Pt/TiO₂. Analogously, Pt/Na_xTiO₂ catalysts also have many structural distinctions with each other. As the pH value increases, the surface area of obtained catalyst decreases and in turn the content of titanate increases. Overall, the internal distinctions among Pt/Na_xTiO₂ catalysts are only the numerical difference.

To our knowledge, the morphological difference between Pt/TiO₂ and Pt/Na_xTiO₂ could not be a main factor for influencing the final catalytic performance under the present evaluation condition. By contrast, the surface area and the surface composition are of relative importance, which can determine the reaction interface size and surface properties, respectively. Both factors are closely related to the adsorption behavior of reactants. Herein, the HCHO-TPD experiment was carried out to study the structural influence of support on the catalytic performance. As shown in Fig. 9, the HCHO-TPD profile of TiO₂ can be also divided into two regions, corresponding to the desorption of HCHO (25–160 °C) and decomposed species (160–400 °C) due to the strong adsorption of HCHO, respectively [53,54]. The HCHO molecules have similar adsorption behavior on NaT2 to that on TiO₂ because their HCHO desorption temperature of NaT2 and TiO₂ are identical. According to the preparation description and XRD results (seen in Fig. 1), it was known that NaT2 was synthesized with low pH value of ion exchange so that Na content on the surface was relatively less, meaning the low amount of generated titanate. Thus, similar surface properties of NaT2 and TiO₂ can explain why their comparable adsorption behavior of HCHO. However, for the rest of the Na_xTiO₂, the desorption peaks of HCHO in high temperature region uniformly shifts towards the low temperature, implying the HCHO adsorption behavior is changed. The HCHO adsorption amount of various catalysts can be estimated by peak area, and the integrated results are listed in

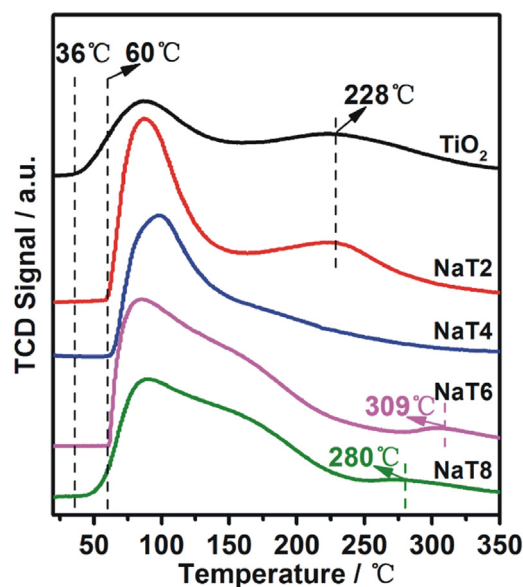


Fig. 9. HCHO-TPD patterns of Na_xTiO₂ and TiO₂ without loading Pt particles.

Table S1 of ESI. Clearly, all the Na_xTiO₂ have higher HCHO adsorption amount than that of TiO₂. Thereinto, the large surface area can account for the high HCHO adsorption amount for NaT2 but could not for other Na_xTiO₂. The HCHO adsorption amount has no monotonous relationship with the surface area of Na_xTiO₂. Especially for NaT8, the HCHO adsorption amount is larger than that of TiO₂, but the surface area is only around half. Hence, besides the surface area, the surface properties should be another key factor for influencing the HCHO adsorption amount. High Na content of NaT4 ~ 8 can provide the superficial alkalinity, which can facilitate the adsorbed HCHO molecules to easily generate quasi-multimer or other condensed state. Note that the HCHO oxidation follows a pseudo-first-order kinetics with respect to the HCHO concentration [55]. This means the reaction rate of various catalysts is subject to the HCHO concentration. That is to say, the enhanced HCHO adsorption can make more HCHO enriched near catalytic sites, decline the diffusion or transfer resistance and finally help to improve the catalytic performance of Pt/Na_xTiO₂.

On the other hand, besides the adsorption behavior of reactants, the surface area and the surface properties of catalytic support can further change the dispersion state of the active species. According to TEM images (seen in Fig. 3), Pt particles on Na_xTiO₂ exhibits smaller average size compared with that on TiO₂, and they become smaller as pH value increases. But the smaller Pt particles on Na_xTiO₂ do not expose more Pt atoms outside according to the CO amount in Table 2. This indicates the Pt/Na_xTiO₂ catalyst should have possessed bad HCHO oxidation performance. Actually, it is not the case here. Thus, the Pt particle size and its exposed state can't respond to different catalytic performance of Pt/Na_xTiO₂ catalysts and Pt/TiO₂. Furthermore, TPR and TPO results (seen in Fig. 6) manifest the metal-support interaction mechanism of Na_xTiO₂-supported Pt catalysts is varied, which directly change the redox properties of Pt particles. As also demonstrated by XPS analysis (seen in Fig. 5), Pt particles on Na_xTiO₂ are liable to be oxidized in form of cationic Ptδ⁺. With respect to which one, metallic or ionic Pt, has the catalytic activity, there are still in debate up to now [15,56–58]. The present results at least prefer to the ionic Pt functional mechanism. In the following, in situ HCHO-DRIFTS experiment was carried out to study the influence of Pt dispersion state on the HCHO catalytic oxidation.

Fig. 10 shows the in situ DRIFTS spectra of catalysts exposed in different atmosphere at ambient temperature under steady

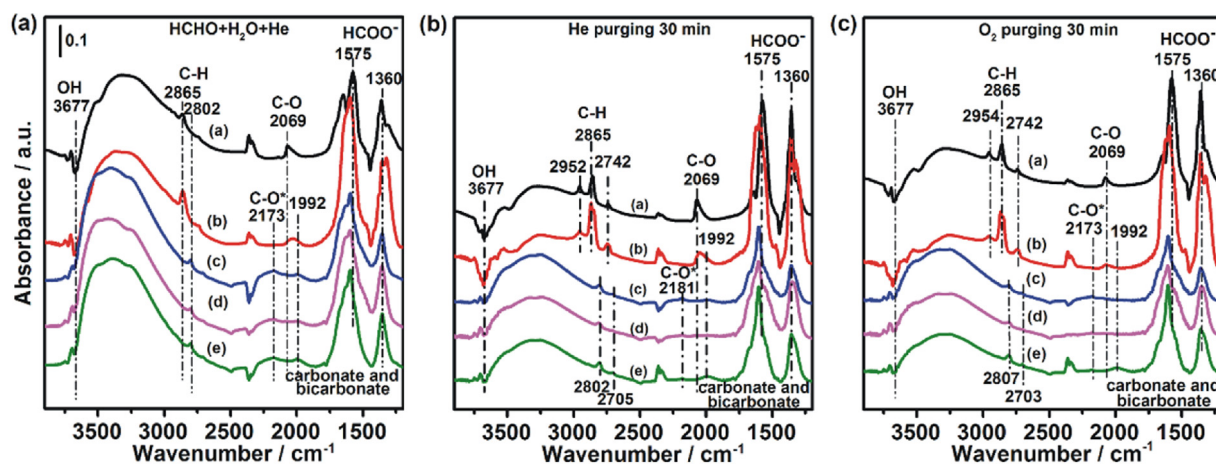


Fig. 10. In situ DRIFTS spectra over Pt/Na_xTiO₂ and Pt/TiO₂ after (a) a flow of He + HCHO + H₂O for 1 h followed by (b) He purging for 30 min, and finally (c) O₂ purging for 30 min at room temperature. The dynamic change of various DRIFTS spectra as a function of time can be seen in Fig. S1 of ESI.

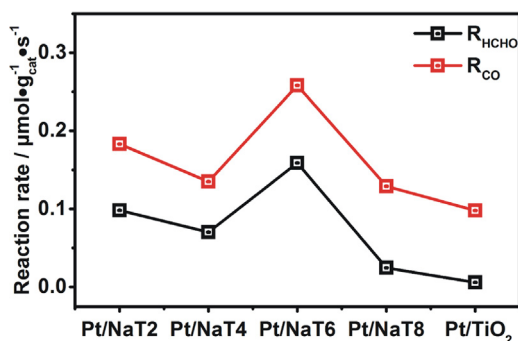


Fig. 11. Reaction rate of CO oxidation (R_{CO}) and HCHO catalytic oxidation (R_{HCHO}) of various catalysts at 30 °C. The CO oxidation conversion can be seen in Fig. S2 of ESI. The GHSV = 12000 ml h⁻¹ g⁻¹.

state. From left to right in order are the catalysts exposed to HCHO + H₂O + He, pure He, and 20% O₂/He. Most studies have found that the catalytic oxidation of formaldehyde on Pt/TiO₂ generally went through DOM, formate, adsorbed CO species to the final products [4]. At the initial stage of HCHO adsorption, it can be seen the signals at 2802 cm⁻¹ and 2865 cm⁻¹ appeared on the spectra as soon as the injection of formaldehyde and water, which is corresponding to the C–H vibrations of DOM [59]. Simultaneously, remarkable peaks at 1575 cm⁻¹ and 1360 cm⁻¹ are attributed to the produce of formate [56,60]. For Pt/TiO₂, the linear adsorption of CO (CO_{liner}) on the Pt surface can be observed at 2058 cm⁻¹. Besides the signals of DOM and formate mentioned above, the curve of Pt/Na_xTiO₂, apart from Pt/Na₂TiO₂, also displays two vibrations at 1992 cm⁻¹ and 2173 cm⁻¹. Corresponding signal intensity continuously strengthens as the pH value of Pt/Na_xTiO₂ increases. The vibration with lower frequency can be assigned to the carbonate/bicarbonate, and the frequency of the latter vibration is similar to that of gaseous CO [61]. We deduce that the interaction of adsorbed CO species with catalyst is weakened on the Pt/Na_xTiO₂, which may be in form of analogical physical adsorption. However, this does not mean the generation of gaseous CO on Pt/Na_xTiO₂ in the practical application process. As shown in Fig. 11, CO oxidation reaction rate of various Pt catalysts is several-fold higher than their HCHO reaction rate under same reaction condition. No CO was detected in exhaust gas during the catalytic activity test in the present studies. At the He gas purge stage, signals located at 2742 cm⁻¹ and 2865 cm⁻¹ are more significant, same tendency as formate signal which vibrate at 1575 cm⁻¹ and 1360 cm⁻¹. The signal of CO_{liner} at 2058 cm⁻¹ on Pt/TiO₂ still exists, but the bumpiness

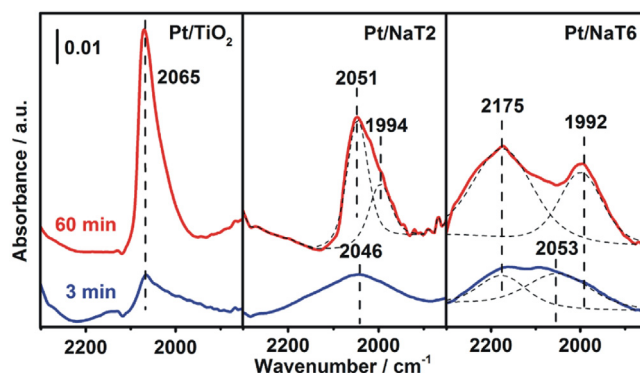


Fig. 12. The qualitative change between 1950 cm⁻¹ and 2200 cm⁻¹ of HCHO-DRIFTS spectra at the initial and saturated adsorption stage.

at 2173 cm⁻¹ on Pt/Na_xTiO₂ disappears rapidly, which demonstrates the weak adsorption for this part of CO molecules. At the last stage, the signal intensity of CO_{liner} is weakened due to the oxidation into CO₂.

Obviously, reaction pathway of Pt/TiO₂ in present work follows the general HCHO decomposition route (HCHO → DOM → formate → CO → CO₂). However, on Pt/Na_xTiO₂, the formate is decomposed into carbonate/bicarbonate and weakly adsorbed CO instead of sole linearly adsorbed CO, and finally oxidized to be CO₂. The generation of carbonate/bicarbonate was considered to be attributed to the direct reaction of formate with hydroxyls that were brought by the alkaline-earth metal species [15]. Further analysis on dynamic changes of DRIFTS spectra, the founding in Fig. 12 displays that linearly adsorbed CO and weakly adsorbed CO are simultaneously appeared on Pt/Na₆TiO₂ at first 3 min. Then, the linearly adsorbed CO is converted to the carbonate/bicarbonate while the weakly adsorbed CO still exists at 60 min. This can demonstrate the formate is firstly decomposed into two kinds of CO, the linearly adsorbed one and weakly adsorbed one, although the presence of abundant hydroxyls. Different phenomenon occurs on Pt/Na₂TiO₂ that only the linearly adsorbed CO are formed at the beginning, a small part of which successively are transformed into the carbonate/bicarbonate. In comparison, Pt/TiO₂ merely has the linearly adsorbed CO that maintains to be still during the HCHO injection process.

As shown in Fig. 13(a), the signal intensity of formate on various catalysts was integrated to semi-quantitatively compare the formate amount as a function of time. Numerous literatures have pointed out that decomposition of formate was the rate-limiting

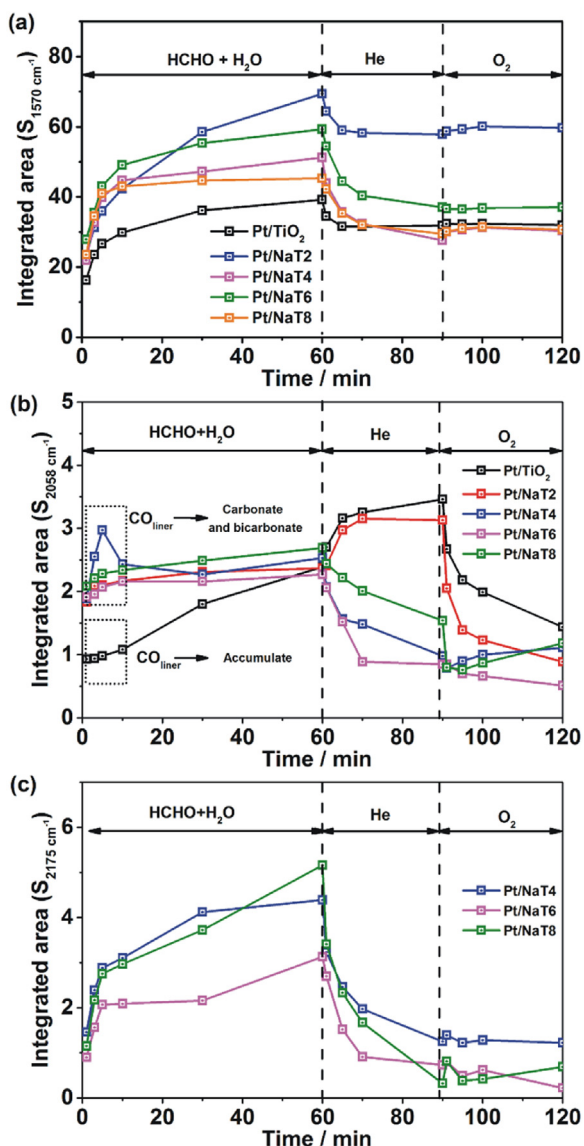


Fig. 13. Integrated results of various peaks as a function of time over Pt/Na_xTiO₂ and Pt/TiO₂.

step of HCHO oxidation [4,62]. It can be seen that the formate starts to acutely accumulate on various catalysts when the HCHO are injected. Even though switch to the He and O₂ purging, the formate amount does not observably decline, implying the slow decomposition of formate that endorses the view of published literatures [4]. DFT calculation results displayed that the formate decomposition had a high energy barrier, which suggested the difficult occurrence in essence compared with other reaction steps of HCHO oxidation. Among several possible reaction routes, reactive O* and OH* involved could assist dehydrogenation of formate and afterwards decomposition [62]. That means the O* and OH* plays important roles in formate decomposition. Accordingly, our XPS analysis results in Table 3 show that both active species of Pt/Na_xTiO₂ are obviously higher than that of Pt/TiO₂, which can be one of reasons accounted for the excellent performance of Pt/Na_xTiO₂.

According to the reaction route mentioned above, the HCHO oxidation is a consecutive reaction. Therefore, the improvements in catalytic performance should be focused on the adsorption and reaction of every intermediate. It is known that CO can strongly adsorb on Pt, which is even considered to be a poison in some catalytic systems, for example methanol electronic catalytic oxidation

[63]. The fundamental issue is that the strong adsorption of CO can inhibit the adsorption and activation of O*, OH* or other species on Pt active sites. The analogous explanation can also be appropriate for the worse CO oxidation performance of Pt/TiO₂ compared with that of Au/TiO₂ [64,65]. Therefore, besides concerning the formate decomposition, it is necessary to pay attention to the CO consumption.

Under normal condition, CO generated from formate decomposition is oxidized by O₂ purging to carry out the reaction progress. Incorporation of hydroxyls brought by alkali species can increase the oxidation rate of CO. As shown in Fig. 13(b), He or O₂ purging fleetly declines the amount of carbonate/bicarbonate on Pt/Na_xTiO₂. By contrast, the amount of CO on Pt/TiO₂ maintains to be relatively high. It can be seen that both strategies for CO consumption are implemented through oxidation reaction. As discussed, if the adsorption strength of CO with Pt particles was weakened, there would be more Pt active sites re-exposure to adsorb or activate other reactants, which further improve the catalytic performance. Fig. 13(c) shows the interaction strength of weak adsorbed CO species with catalyst indeed is not strong that they can be vanished after He or O₂ purging. Exactly as shown in Fig. 11, the catalyst with appearance of weak-adsorbed CO has both good CO oxidation performance and high HCHO oxidation rate.

Based on the results and discussion mentioned above, three possible reaction routes of HCHO catalytic decomposition over Pt/Na_xTiO₂ are proposed, as schematically illustrated in Fig. 14. First two steps of HCHO oxidation reaction, the transformation of HCHO into formate via DOM, are same on various Pt/Na_xTiO₂. However, the following progress from formate to CO₂ has different routes relying on the pH value of Pt/Na_xTiO₂. Over Pt/Na₂TiO₂, the formate is firstly converted to the linearly adsorbed CO. Note that one part of linearly adsorbed CO are oxidized by active oxygen species into CO₂ as follows the reaction path 1, which is also the route of HCHO oxidation over Pt/TiO₂ catalyst. The rest CO, abided by the reaction path 2, are reacted with hydroxyls to form the carbonate/bicarbonate and finally be dehydrated to be CO₂. That is to say, there are two possible reaction routes for HCHO decomposition coexisted on Pt/Na₂TiO₂. As the pH value of catalysts increases, the formate on corresponding Pt/Na_xTiO₂ is transformed into two kinds of CO, the linearly adsorbed one and the weakly adsorbed one. The reaction mechanism of linearly adsorbed CO follows the reaction path 2, and the weakly adsorbed CO would be also reacted with active oxygen species to form CO₂ as described in the reaction path 3. According to the catalytic performance data mentioned above, it is confirmed that the HCHO oxidation reaction following the path 2 and 3 can exhibit more significant efficiency than the reaction path 1.

4. Conclusions

In summary, the present work demonstrated that the titania nanowire containing sodium was a kind of excellent support for HCHO catalytic oxidation. Pt particles on these materials can be well dispersed and easily oxidized. The corresponding catalysts can have several times promoted activity at room temperature compared with pure TiO₂-supported catalyst. The good affinity of catalyst with HCHO and the alteration of reaction pathway were considered to be two main factors responsible for the enhanced catalytic performance.

Acknowledgements

This work was supported financially by the National Natural Science Foundation of China (21406118, 91434109, 91334202), the Highly Educated Talent Foundation of Nanjing Forestry University (GXL2014036), Jiangsu graduate scientific research and innovation

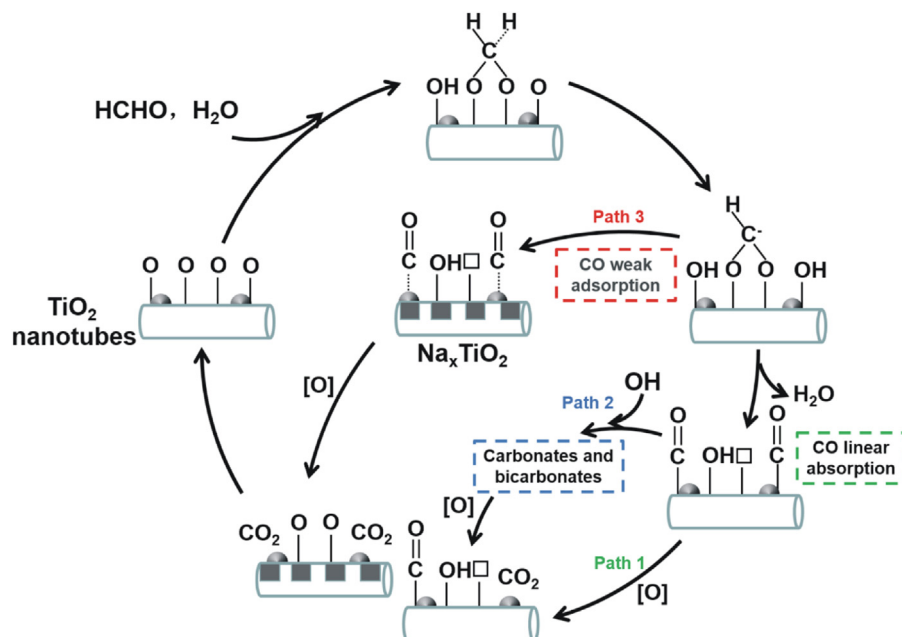


Fig. 14. Scheme for the catalytic oxidation process of formaldehyde over various Pt/Na_xTiO₂ catalysts.

projects (KYLX16-0842), Priority Academic Program Development of Jiangsu Higher Education Institutions.

Appendix A. Supplementary data

Supplementary data associated with this article can be found, in the online version, at <http://dx.doi.org/10.1016/j.apcatb.2017.07.073>.

References

- [1] J.J. Collins, N.A. Esmen, T.A. Hall, *Am. J. Ind. Med.* 39 (2001) 336–345.
- [2] L.F. Wang, M. Sakurai, H. Kameyama, *J. Hazard. Mater.* 167 (2009) 399–405.
- [3] L.F. Wang, Q. Zhang, M. Sakurai, H. Kameyama, *Catal. Commun.* 8 (2007) 2171–2175.
- [4] C.B. Zhang, H. He, *Catal. Today* 126 (2007) 345–350.
- [5] J.X. Peng, S.D. Wang, *J. Phys. Chem. C* 111 (2007) 9897–9904.
- [6] N.H. An, P. Wu, S.Y. Li, M.J. Jia, W.X. Zhang, *Appl. Surf. Sci.* 285 (2013) 805–809.
- [7] X.F. Zhu, B. Cheng, J.G. Yu, W.K. Ho, *Appl. Surf. Sci.* 364 (2016) 808–814.
- [8] Z.P. Qu, D. Chen, Y.H. Sun, Y. Wang, *Appl. Catal. A: Gen.* 487 (2014) 100–109.
- [9] X.W. Hong, Y. Sun, T.L. Zhu, Z.M. Liu, *Catal. Sci. Technol.* 6 (2016) 3606–3615.
- [10] H.B. Na, T.L. Zhu, Z.M. Liu, *Catal. Sci. Technol.* 4 (2014) 251–257.
- [11] X.H. Yu, J.H. He, D.H. Wang, Y.C. Hu, H. Tian, T.X. Dong, Z.C. He, *J. Nanopart. Res.* 14 (2012).
- [12] Y. Wang, C.Y. Dai, B.B. Chen, Y.D. Wang, C. Shi, X.W. Guo, *Catal. Today* 258 (2015) 616–626.
- [13] Y.C. Huang, H.B. Li, M. Balogun, H. Yang, Y.X. Tong, X.H. Lu, H.B. Ji, *RSC Adv.* 5 (2015) 7729–7733.
- [14] X.H. Yu, J.H. He, D.H. Wang, Y.C. Hu, H. Tian, Z.C. He, *J. Phys. Chem. C* 116 (2012) 851–860.
- [15] C.B. Zhang, F.D. Liu, Y.P. Zhai, H. Ariga, N. Yi, Y.C. Liu, K. Asakura, M. Flytzani-Stephanopoulos, H. He, *Angew. Chem. Int. Ed.* 51 (2012) 9628–9632.
- [16] Z.X. Yan, Z.H. Xu, J.G. Yu, M. Jaroniec, *Appl. Catal. B: Environ.* 199 (2016) 458–465.
- [17] T.F. Yang, Y. Huo, Y. Liu, Z.B. Rui, H.B. Ji, *Appl. Catal. B: Environ.* 200 (2017) 543–551.
- [18] J.X. Peng, S.D. Wang, *Appl. Catal. B: Environ.* 73 (2007) 282–291.
- [19] L. Zhu, J.L. Wang, S.P. Rong, H.Y. Wang, P.Y. Zhang, *Appl. Catal. B: Environ.* 211 (2017) 212–221.
- [20] J. Zhou, L.F. Qin, W. Xiao, C. Zeng, N. Li, T. Lv, H. Zhu, *Appl. Catal. B: Environ.* 207 (2017) 233–243.
- [21] S.J. Tauster, S.C. Fung, R.L. Garten, *J. Am. Chem. Soc.* 1 (1978) 170–175.
- [22] A.E.R. Mohamed, S. Rohani, *Energ. Environ. Sci.* 4 (2011) 1065–1086.
- [23] D.P. Macwan, P.N. Dave, S. Chaturvedi, *J. Mater. Sci.* 46 (2011) 3669–3686.
- [24] W. Li, Z.X. Wu, J.X. Wang, A.A. Elzatahy, D.Y. Zhao, *Chem. Mater.* 26 (2014) 287–298.
- [25] T. Kasuga, M. Hiramatsu, A. Hoson, *Langmuir* 14 (1998) 3160–3163.
- [26] H. Izawa, S. Kikkawa, M. Koizumi, *J. Phys. Chem.* 86 (1982) 5023–5026.
- [27] L.C. Li, T.T. He, X.J. Zhao, Q. Qian, L. Wang, X.B. Li, *J. Inorg. Mater.* 31 (2016) 1198–1204.
- [28] H.M. Li, K.L. Wang, W. Li, S.J. Cheng, K. Jiang, *J. Mater. Chem. A* 3 (2015) 16495–16500.
- [29] H.F. Xu, C.X. Li, D.W. He, Y.B. Jin, *Powder Diff.* 29 (2014) 147.
- [30] C.L. Wong, Y.N. Tan, A.R. Mohamed, *J. Environ. Manage.* 92 (2011) 1669–1680.
- [31] L.C. Li, Y.F. Wang, K.Z. Shi, S.S. Chen, Z.H. Yang, X.H. Lu, *Catal. Lett.* 142 (2012) 480–485.
- [32] X.L. Zhu, M. Shen, L.L. Lobban, R.G. Mallinson, *J. Catal.* 278 (2011) 123–132.
- [33] P. Panagiotopoulou, D.I. Kondarides, *J. Catal.* 260 (2008) 141–149.
- [34] G.S. Lane, E.E. Wolf, *J. Catal.* 105 (1987) 386–404.
- [35] J. Ruiz-Martínez, A. Sepúlveda-Escribano, J.A. Anderson, F. Rodríguez-Reinos, *Phys. Chem. Chem. Phys.* 11 (2009) 917–920.
- [36] M.Q. Shen, L.F. Lv, J.Q. Wang, J.X. Zhu, Y. Huang, J. Wang, *J. Chem. Eng.* 255 (2014) 40–48.
- [37] B. Qiao, A. Wang, X. Yang, L.F. Allard, Z. Jiang, Y. Cui, J. Liu, J. Li, T. Zhang, *Nat. Chem.* 3 (2011) 634–641.
- [38] H.B. Huang, D.Y.C. Leung, *J. Catal.* 280 (2011) 60–67.
- [39] H.B. Huang, D.Y.C. Leung, *ACS Catal.* 1 (2011) 348–354.
- [40] Y.B. Li, C.B. Zhang, H. He, *Catal. Today* 281 (2017) 412–417.
- [41] Y.B. Li, C.B. Zhang, H. He, J.H. Zhang, M. Chen, *Catal. Sci. Technol.* 6 (2016) 2289–2295.
- [42] B.Y. Bai, J.H. Li, *ACS Catal.* 4 (2014) 2753–2762.
- [43] H.Y. Chen, M.N. Tang, Z.B. Rui, H.B. Ji, *Ind. Eng. Chem. Res.* 54 (2015) 8900–8907.
- [44] R. Fiala, A. Figueroba, A. Bruix, M. Vaclav, A. Rednyk, I. Khalakhan, M. Vorokhta, J. Lavkova, F. Illas, V. Potin, I. Matolinova, K.M. Neyman, V. Matolin, *Appl. Catal. B: Environ.* 197 (2016) 262–270.
- [45] R. Würz, M. Rusu, T. Schedel-Niedrig, M.C. Lux-Steiner, H. Bluhm, M.H. Vecker, E. Kleimenov, A. Knop-Gericke, R. Schl. Gl., *Surf. Sci.* 580 (2005) 80–94.
- [46] C.Q. Zhu, A. Osherov, M.J. Panzer, *Electrochim. Acta* 111 (2013) 771–778.
- [47] M. Yang, J.L. Liu, S. Lee, B. Zugic, J. Huang, L.F. Allard, M. Flytzani-Stephanopoulos, *J. Am. Chem. Soc.* 137 (2015) 3470–3473.
- [48] H.N. Evin, G. Jacobs, J. Ruiz-Martínez, U.M. Graham, A. Dozier, G. Thomas, B.H. Davis, *Catal. Lett.* 122 (2008) 9–19.
- [49] P. Panagiotopoulou, A. Christodoulakis, D.I. Kondarides, S. Boghosian, *J. Catal.* 240 (2006) 114–125.
- [50] E. Morgado, J.L. Zotin, M.A.S. de Abreu, D.D.O. Rosas, P.M. Jardim, B.A. Marinkovic, *Appl. Catal. A: Gen.* 357 (2009) 142–149.
- [51] X.B. Chen, H.Q. Wang, S. Gao, Z.B. Wu, *J. Colloid Interf. Sci.* 377 (2012) 131–136.
- [52] C.H. Lin, J.H. Chao, W.J. Tsai, M.J. He, T.J. Chiang, *Phys. Chem. Chem. Phys.* 16 (2014) 23743–23753.
- [53] S. Colussi, M. Boaro, L. de Rogatis, A. Pappacena, C. de Leitenburg, J. Llorca, A. Trovarelli, *Catal. Today* 253 (2015) 163–171.
- [54] Y.B. Li, C.B. Zhang, J.Z. Ma, M. Chen, H. Deng, H. He, *Appl. Catal. B: Environ.* 217 (2017) 560–569.
- [55] L.F. Qi, B. Cheng, J.G. Yu, W.K. Ho, *J. Hazard. Mater.* 301 (2016) 522–530.
- [56] H.B. Huang, D.Y.C. Leung, D.Q. Ye, *J. Mater. Chem.* 21 (2011) 9647–9652.
- [57] N.H. An, W.L. Zhang, X.L. Yuan, B. Pan, G. Liu, M.J. Jia, W.F. Yan, W.X. Zhang, *Chem. Eng. J.* 215–216 (2013) 1–6.
- [58] Z.X. Yan, Z.H. Xu, J.G. Yu, M. Jaroniec, *Environ. Sci. Technol.* 49 (2015) 6637–6644.

- [59] C.F. Mao, M.A. Vannice, *J. Catal.* 154 (1995) 230–244.
- [60] C.B. Zhang, H. He, K. Tanaka, *Appl. Catal. B: Environ.* 65 (2006) 37–43.
- [61] P.A. Sermon, V.A. Self, E.P.S. Barrett, *J. Mol. Catal.* 65 (3) (1991) 377–384.
- [62] S.R. Li, X.Q. Lu, W.Y. Guo, H.Y. Zhu, M. Li, L.M. Zhao, Y. Li, H.H. Shan, *J. Organomet. Chem.* 704 (2012) 38–48.
- [63] Y.M. Zhu, H. Uchida, T. Yajima, M. Watanabe, *Langmuir* 17 (2001) 146–154.
- [64] H. Kung, *J. Catal.* 216 (2003) 425–432.
- [65] M. Haruta, *Stud. Surf. Sci. Catal.* 110 (1997) 123–134.